Marine Pollution Bulletin 189 (2023) 114729

Contents lists available at ScienceDirect

Marine Pollution Bulletin

journal homepage: www.elsevier.com/locate/marpolbul

The dynamics of biofouled particles in vortical flows

Hannah Kreczak, Andrew W. Baggaley *, Andrew J. Willmott

Newcastle University, UK

ARTICLE INFO

Keywords:
Microplastic
Biofouling
Turbulence

ABSTRACT

When using mathematical models to predict the pathways of biofouled microplastic in the ocean, it is necessary to parametrise the impact of turbulence on their motions. In this paper, statistics on particle motion have been computed from simulations of small, spherical particles with time-dependent mass in cellular flow fields. The cellular flows are a prototype for Langmuir circulation and flows dominated by vortical motion. Upwelling regions lead to particle suspension and particles fall out at different times. The uncertainty of fallout time and a particle's vertical position is quantified across a range of parameters. A slight increase in settling velocities, for short times, is observed for particles with inertia due to clustering in fast downwelling regions for steady, background flow. For particles in time-dependent, chaotic flows, uncertainty is significantly reduced and we observe no significant increase in the average settling rates due to inertial effects.

1. Introduction

Marine plastic pollution is of high societal concern, identified as a major global conservation issue impacting marine life, human health, and maritime industries (Napper and Thompson, 2020; Davison et al., 2021). Microplastics, which are defined as plastic particles with a diameter between 1 μm and 5 mm (Andrady, 2011), are ubiquitous in the marine environment and due to their size they can be easily ingested by marine fauna with detrimental affects on their health (Cole et al., 2013; Wright et al., 2013). Primary sources for microplastic pollution include cosmetic micro-beads and clothing microfibres in wastewater, while secondary sources are the results of large plastic waste fragmenting into smaller pieces through the action of degradation (Avio et al., 2017). Theoretical fragmentation models hypothesise that the number of particles of a given size increases exponentially as the particle size decreases (Cózar et al., 2014; Eriksen et al., 2014).

With 62 % of plastics produced made of buoyant material compared to seawater (Andrady, 2011), it is sensible to presume a large portion of microplastics would be found floating in the ocean. However, empirical measurements are less than expectation (Cózar et al., 2014; Eriksen et al., 2014; Van Sebille et al., 2015), and observations have found buoyant microplastics dispersed throughout the ocean water column and in the sea-floor sediment (Li et al., 2020; Int-Veen et al., 2021). Several processes have been attributed to the transport of buoyant plastics from surface waters to these sub-surface locations, including transport in faecal pellets following ingestion by marine fauna (Kvale et al., 2020), entrainment in marine snow (Kvale et al., 2020; Porter et al., 2018), or colonization by micro-organisms and algae (biofouling) (Kvale et al., 2020; Rummel et al., 2017), the latter being the focus of the study here-on in.

Submerged surfaces in the ocean quickly gain micro-organisms, the collection of which is known as a biofilm (Salta et al., 2013). It has been widely reported that the surface of marine plastics are susceptible to acquiring biofilms, which can be made up of bacteria, algae, and crustaceans (Ye and Andrady, 1991; Fazey and Ryan, 2016; Kaiser et al., 2017; Michels et al., 2018). Biofilms have the capacity to influence the fate of microplastics by modifying the hydrophobicity and buoyancy of the plastics they inhabit (Van Melkebeke et al., 2020). Empirical and experimental studies have analysed the initial sinking behaviour of biofouled microplastics in aquatic environments, finding microplastics can become sufficiently fouled enough to sink in both the ocean (Ye and Andrady, 1991; Fazey and Ryan, 2016; Kaiser et al., 2017) and freshwater lakes (Lagarde et al., 2016; Chen et al., 2019), in as little as 2 weeks after exposure (Fazey and Ryan, 2016). The rate of biofouling and whether a fouled particle becomes negatively buoyant depends on geographical location (Kaiser et al., 2017) and seasonal effects (Chen et al., 2019). However, these studies are unable to comment on the long-time fate of the microplastics once they have left the ocean surface, which is necessary to quantify their impact in the marine environment.

Observing the transport of biofouled microplastics once they have sunk is difficult, therefore, mathematical models capturing ocean velocities, particle hydrodynamics, and biofilm population dynamics are

* Corresponding author.
E-mail address: Andrew.Baggaley@Newcastle.ac.uk (A.W. Baggaley).

https://doi.org/10.1016/j.marpolbul.2023.114729
Received 7 December 2022; Received in revised form 8 February 2023; Accepted 9 February 2023

essential to predict 3D transport of microplastics in the ocean. Deterministic models capturing the one-dimensional, subsurface vertical motion of biofouled particles in ambient oceans have been studied. Kooi et al. (2017) developed a detailed model for spherical plastic particles with an even biofilm coating. The model predicted aperiodic, subsurface oscillations where particles rarely, if ever, resurfaced. Kreczak et al. (2021) extracted the salient dynamics of the Kooi et al. model (Kooi et al., 2017) and determined the governing mechanisms of the particle's long-time motion identifying that large concentrations of microplastics are expected to be within a subsurface layer bounded by the euphotic and pycnocline depths. Both of these models neglected the effects of ocean velocity on the microplastic motion.

Several models have investigated the transport and resulting distribution of biofouled or negatively buoyant microplastics in 3D ocean general circulation models (OGCMs) (Mountford and Morales Maqueda, 2019; Jalón-Rojas et al., 2019; Lobelle et al., 2021; Fischer et al., 2022). In all the models, large-scale horizontal and vertical motions are resolved. Sub-grid turbulent fluid motion is parametrised via eddy diffusivity, either as a term in a Eulerian framework (Mountford and Morales Maqueda, 2019), simulated as a random walk in the Lagrangian framework (Jalón-Rojas et al., 2019; Fischer et al., 2022), or neglect turbulence entirely (Lobelle et al., 2021). Since eddy diffusivity coefficients do not capture the spatio-temporal complexity of oceanic turbulence, the predictions of particle trajectories in these models may be inaccurate. This is the motivation behind the study presented here, where we have made a first-step in investigating the potential impact of oceanic sub-grid scale flows on biofouled microplastic transport. In this study we focus on cellular flows, as a prototype for both Langmuir circulations and turbulent flows dominated by vortical motion. A comprehensive discussion on the different processes that govern the transport of floating marine plastic debris in the ocean can be found in the review of Van Sebille et al. (2020).

Langmuir circulations are coherent, cellular rolls aligned with the wind that occur in the upper ocean. They are generated by an instability arising from the interaction between Stokes drift transport and the wind-induced current. They are powerful mechanisms for vertical mixing in the ocean, with typical depth and horizontal spacing of 4–6 and 10–50 m, respectively (Talley, 2011), and maximum vertical velocities of between 2 and 10 $cm{\cdot}s^{-1}$ (Leibovich, 1983), and can persist for a number of days (Li et al., 2013). Typical streamlines of a pair of cells in Langmuir turbulence are depicted in Fig. 1. In contrast, the smallest turbulent vortices we consider are on the order of centimetres, which can be thought of as the smallest scale vortices in the inertial range of multi-scale turbulence processes which can generate a deep mixed-layer depth, such as the wind-shear and internal wave mixing depicted in Fig. 1. The turbulent processes depicted in Fig. 1 are just a representative

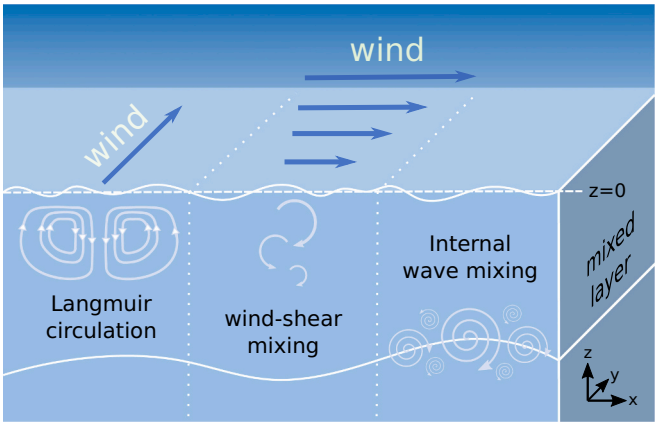

Fig. 1. Illustrative sketch of sub-grid ocean turbulent processes of interest to the study herein. $z = 0$ represents the mean sea-surface and scales are not representative of reality.

subset, and is far from an exhaustive representation of all the sub-mesoscale turbulent processes which impact plastic transport (Van Sebille et al., 2020).

Fluid flows can have significant effect on particle transport and their settling rates. In an idealised model representing plankton in Langmuir circulation, Stommel (1949) identified that negatively buoyant, passive particles could become indefinitely suspended in upwelling regions of a vortical flow. For aerosol particles, which are small, heavy, spherical particles with inertia, it is observed that all particles will eventually settle-out in vortical flows since the vortical nodes become unstable (Maxey and Corrsin, 1986; Maxey, 1987). These heavy, inertial particles cluster onto closed curves, favouring downwelling regions, and consequently there is an increase in the particle settling velocity compared to no fluid flow. This is also the case for isotropic, homogenous turbulence where up to 50 % increase on settling velocity is reported for heavy aerosol particles (Wang and Maxey, 1993). In contrast, for positively buoyant, small particles, such as bubbles, vortical centres can act as stable trapping regions (Maxey, 1987). During biofilm growth a microplastic-biofilm aggregate will transition from positive to negative buoyancy, therefore, transitioning from the bubble to aerosol regime. In addition, an aggregate will be expected to interact with a large variety of sub-grid, multi-scale ocean flows as they are transported. The literature suggests that for particles in vortical flows we would expect some suspension in the early stages and clustering in later stages due to inertia, the former delaying settling and the latter resulting in increased settling velocity. These aforementioned studies lead us to conclude that we cannot heuristically predict the impact turbulent fluid flows have on the motion of biofouled microplastics.

We investigate the motion of biofouled microplastic in sub-grid oceanic flows by simulating the motion of spherical particles with time-dependent mass in two-dimensional, deterministic cellular flow composed of a periodic array of counter-rotating vortices. We model the microplastic-biofilm aggregates in the flow field as small, spherical particles with a uniform biofilm covering. Although most microplastics collected from the marine environment are non-spherical, this initial study is appropriate to understand the simplest model of particles with time varying buoyancy in vortical flows. We also assume the concentration of particles is low enough that they do not modify the flow or interact with each other, which would be expected of microplastics highly dispersed in the ocean.

We statistically analyse the motion of many particles, initially distributed throughout a vortex cell whose top boundary resides at the sea-surface, as a prototype for Langmuir circulation cells or vortical turn-overs associated with wind-driven mixing (Fig. 1). We track particle trajectories during suspension and following fallout from the vortical cell. Analysing the motion of many particles helps to obtain a complete understanding of average particle motion and particular attention will be paid to the uncertainty these vortical-like flows can introduce into particle fall-out rates. We emphasise that the model developed here does not directly capture oceanic turbulent conditions, and instead the simple system elucidates the sinking behaviours of small particles with time-dependent mass and how they respond to non-uniform flow. This will increase understanding when considering the settling motion of particles with increasing mass in more computational demanding, complex flows, such as direct numerical simulation of multi-scale 3D turbulent flows.

2. Model development

2.1. Motion of small particles in cellular flow

The trajectory of a small, spherical particle in fluid flow moves according to the Maxey-Riley-Gatignol equations (Maxey and Riley, 1983; Gatignol, 1983). We model the system as two-dimensional, taking x to represent the horizontal direction and z the vertical, taking z=0 to represent the mean sea-surface such that the fluid domain is $z \leq 0$.

Ignoring Faxen Corrections and the Bassett History term as in (Maxey, 1987), the equations of motion for the centre $\mathbf{r} = (x, z)$ of a particle of radius a [m] and mass m_p [kg] is prescribed by

$$\ddot{\mathbf{r}} = \frac{6\pi a\mu}{m_p + \frac{1}{2}m_f}\left[\mathbf{u}(\mathbf{r}(t), t) - \dot{\mathbf{r}}(t) + \frac{(m_p - m_f)}{6a\pi\mu}\mathbf{g}\right] + \frac{m_f}{m_p + \frac{1}{2}m_f}\left(\mathbf{u} + \frac{1}{2}\dot{\mathbf{r}}\right)\cdot\nabla\mathbf{u}, \tag{1}$$

where $\mathbf{u} = (u_x, u_z)$ is the background fluid velocity [m·s^{-1}], μ is the dynamic viscosity of the fluid, m_f is the mass of fluid displaced by the particle [kg], and gravity is taken to act in the vertical direction such that $\mathbf{g}$=(0, $-$ g), where g is gravitational acceleration [m·s^{-2}]. The components of particle velocity will be denoted $\dot{\mathbf{r}} = (V_x, V_z)$ [m·s^{-1}].

For the flow field $\mathbf{u}$ we take the cellular, Taylor-Green vortex flow with reference coordinates $\mathbf{r} = (x, z)$, given by the streamfunction

$$\psi(x, z) = U_0 L sin\left(\frac{x}{L}\right) sin\left(\frac{z}{L}\right). \tag{2}$$

This flow is a simple representation of Langmuir circulation or convection cells with free-slip boundaries, and has been used as a starting model to study particle motion in homogeneous and isotropic turbulence (Maxey and Corrsin, 1986; Maxey, 1987). The flow is incompressible, and typical streamlines and velocity profiles are shown in Fig. 2(a). The maximum flow speed U_0 for each cell occurs on the cell boundaries, with stagnation points at the centre and corners of each cell. Given the flow has only 2 degrees of freedom, it is not chaotic. The velocity components $\mathbf{u} = (u_x, u_z)$ of Taylor-Green vortices associated with the stream function (2) are

$$u_x = \frac{\partial\psi}{\partial z} = U_0 sin\left(\frac{x}{L}\right) cos\left(\frac{z}{L}\right), \qquad u_z = -\frac{\partial\psi}{\partial x} = -U_0 cos\left(\frac{x}{L}\right) sin\left(\frac{z}{L}\right). \tag{3}$$

The Maxey-Riley-Gatignol equations (Maxey and Riley, 1983; Gatignol, 1983) are valid for small particles at low Reynolds number, provided

$$a/L \ll 1, \quad aW^*\rho_f/\mu \ll 1, \quad a^2 U_0 \rho_f / L\mu \ll 1, \tag{4}$$

based on the cellular flow field scales U_0 [m·s^{-1}] and L [m], and the particle settling velocity $W^* = (m_p - m_f)g/6a\pi\mu$ [m·s^{-1}].

2.2. Particles with time-dependent mass

The focus of this study is to probe the impact of fluid flow on the sinking of the microplastic-biofilm aggregates at the ocean-surface, where it is assumed there is sufficient light and nutrients for the biofilm to grow. Many have reported on the time it takes for a biofilm to grow sufficiently large enough for neutral buoyancy to occur (Kooi et al., 2017; Lobelle et al., 2021). Therefore, we will begin to address what happens after this occurs and consider the dynamics of microplastic-biofilm aggregates once they have achieved neutral buoyancy.

We introduce time dependency in the mass of the particle $m_p(t)$, but model the particle radius as constant. Realistically, biofilm growth would increase the microplastic-biofilm aggregate size, however, as the simplest approximation we assume that the particle radius does not change, but rather the biofilm growth behaves as a pseudo-density change for the particle. This makes the model more tractable for this initial study. We incorporate time-dependency of particle mass as

$$m_p(t) = m_{mp} + N(t)m_{sa}, \tag{5}$$

where m_{mp} is the mass of the clean plastic particle, m_{sa} is the mass of a cluster of biofilm micro-organisms, and $N(t)$ is the number of micro-organism clusters at time t. Replacing m_p in Eq. (1) with Eq. (5) results in the particle motion governed by

$$\ddot{\mathbf{r}} = \frac{1}{\left(1 + N\dfrac{m_{sa}}{m_{mp} + \frac{1}{2}m_f}\right)}\frac{6\pi a\mu}{\left(m_{mp} + \frac{1}{2}m_f\right)}\left[\mathbf{u} - \dot{\mathbf{r}} + \frac{(m_{mp} - m_f)}{6\pi a\mu}\left(1 - \frac{N}{\overline{N}}\right)\mathbf{g}\right] + \frac{1}{\left(1 + N\dfrac{m_{sa}}{m_{mp} + \frac{1}{2}m_f}\right)}\frac{m_f}{\left(m_{mp} + \frac{1}{2}m_f\right)}\left(\mathbf{u} + \frac{1}{2}\dot{\mathbf{r}}\right)\cdot\nabla\mathbf{u}, \tag{6}$$

where

$$\overline{N} = \frac{m_f - m_{mp}}{m_{sa}}, \tag{7}$$

the value of the biofilm population number at which the biofouled particle achieves neutral buoyancy with the surrounding fluid. The biofilm population we model through simple exponential growth

$$N(t) = N_0 exp(\lambda_G t), \tag{8}$$

parameterised by λ_G [s^{-1}], which would be expected for biofilms with sufficient warmth, light exposure, and nutrients at the ocean surface. We initiate particles with a biofilm large enough to achieve neutral buoyancy such that $N(0) \equiv N_0 = \overline{N}$ and model N as continuous since in general $\overline{N}$ is not an integer. More complex deterministic models of biofilm growth dynamics on microplastic throughout the ocean vertical

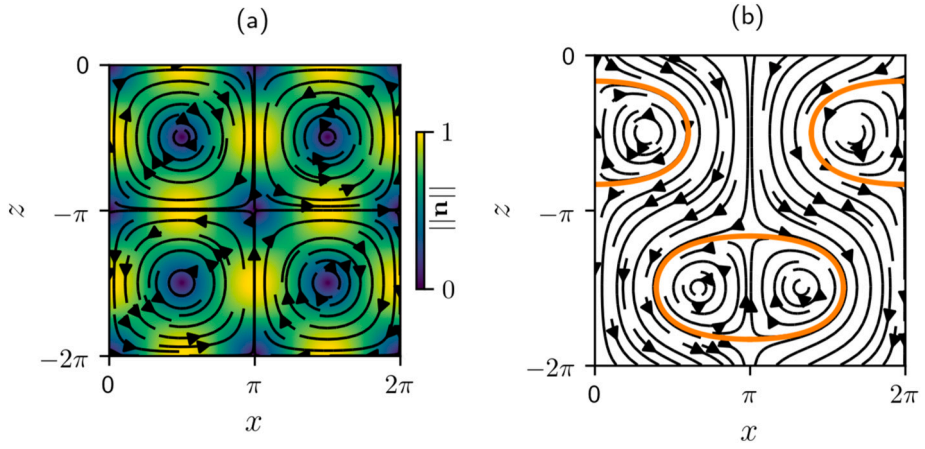

Fig. 2. (a) Velocity profile and streamlines are shown for the periodic cellular flow field governed by Eq. (2). (b) Streamlines representing the trajectories of non-inertial particles in the cellular flow with constant, non-dimensional Stokes settling velocity $\overline{W} = 0.5$. The bounding streamline of the recirculation zones is marked (orange). (For interpretation of the references to colour in this figure legend, the reader is referred to the web version of this article.)

Table 1
Dimensional and non-dimensional parameter ranges relating to buoyant microplastics and oceanic turbulence.

Symbol	Dim parameter name	Oceanic range	Non-dim parameters	Range
ρ_f	Surface ocean density [kg·m^{-3}]	1022–1027	W	10^{-4}–1600
ρ_{mp}	Plastic density [kg·m^{-3}]	840–940		
a	Plastic particle radius [m]	$10^{-5} - 2.5 \times 10^{-3}$	F	500–150,000
λ_G	Algal maximum growth rate [s^{-1}]	2.1×10^{-6}–1.3×10^{-5}		
μ	Dynamic viscosity [kg·m^{-1}·s^{-1}]	10^{-3}–2×10^{-3}	G	0.0001–0.0006
g	Gravitational acceleration [m·s^{-2}]	9.81		
U_0	Vortical velocity scale [m·s^{-1}]	0.001–0.1	D	0.704–0.79
L	Vortical length scale [m]	0.01–5		
ε	Rate of energy dissipation [cm^2·s^{-3}]	10^{-3}–1	M	0.057–0.138
			St	10^{-8}–10^{3}

column have been proposed (Kooi et al., 2017). In this study we are simply interested in the interaction of the aggregates with background fluid flow in the upper ocean for which Eq. (8) suffices.

Considering the background velocity field (Eq. (3)), a particle's equations of motion (Eq. (6)), and biofilm growth condition (Eq. (8)), we choose the following non-dimensional variables, denoted by an asterisk:

$$\mathbf{r} = L\mathbf{r}^*, \quad \mathbf{u} = U_0\mathbf{u}^*, \quad t = \frac{L}{U_0}t^*, \quad N = \overline{N}N^*. \tag{9}$$

The scaled forms of Eqs. (3) and (6) are respectively

$$u_x = sin(x)cos(z), \qquad u_z = -cos(x)sin(z), \tag{10}$$

and

$$\ddot{\mathbf{r}} = \frac{1}{St}\left[\frac{1}{1+MN_0exp(Gt)}\right][\mathbf{u} - \dot{\mathbf{r}} + W(1 - N_0exp(Gt))\hat{\mathbf{z}}] + \frac{D}{1+MN_0exp(Gt)}\left(\mathbf{u} + \frac{1}{2}\dot{\mathbf{r}}\right)\cdot\nabla\mathbf{u}, \tag{11}$$

after dropping the asterisks. The non-dimensional parameters characterising the particle motion are

$$\frac{1}{St} = \frac{9\mu L}{2a^2\left(\rho_{mp} + \frac{1}{2}\rho_f\right)U_0}, \quad D = \frac{\rho_f}{\rho_{mp} + \frac{1}{2}\rho_f}, \quad W = \frac{2(\rho_f - \rho_{mp})ga^2}{9\mu U_0}, \quad M = \frac{\rho_f - \rho_{mp}}{\rho_{mp} + \frac{1}{2}\rho_f}, \quad G = \frac{L/U_0}{\lambda_G^{-1}} \tag{12}$$

where St is the Stokes number, D parameterises the added mass, W is the dimensionless rise velocity of a clean particle, M is the ratio of the density difference of a clean particle and the surrounding fluid to the added mass variation, and G is the quotient between the cellular turnover time and biofilm growth rate. The masses m have been replaced with m=$(4\pi a^3\rho)/3$, where ρ is the respective density [kg·m^{-3}] of each component.

Both the Stokes number St and rise velocity W are dependent on the particle size. To account for this coupling, we rewrite the Stokes number as

$$\frac{1}{St} = \frac{FM}{W}, \quad F = \frac{gL}{U_0^2} = \left(\frac{\sqrt{gL}}{U_0}\right)^2, \tag{13}$$

where we have defined a new dimensionless parameter F. We do this so that only W is defined by the particle radius a, which will vary over orders of magnitude. The parameter F, which is a ratio of speeds U_0 and $\sqrt{gL}$, is a convenient way to change the effective length scale of the cellular flow field. We fix the parameters D and M for typical values of sea water and plastic particle density. The parameter G will also be varied for complete understanding of the particle trajectories. The total range of the dimensional and non-dimensional parameters relevant to biofouled, buoyant microplastic in oceanic turbulence are listed in Table 1. Further discussion on the chosen parameter ranges of our study is given in the Supporting information.

The non-dimensional initial population number is N_0=1, and we investigate initial particle positions (x_0, z_0) throughout the domain Ω=$[0,\pi] \times [-\pi,0]$. This box is chosen as it represents one vortical cell directly below the ocean surface. Many initial points are simulated as the fate of the particles behaviour prior to reaching neutral buoyancy is unknown, since wind-driven mixing can entrain buoyant microplastics into the water column. We statistically analyse the motion of 1000 particles, initiated throughout Ω using a Latin square method to select pairs (x_0, z_0) from 1000 equally spaced $x_0 \in [0,\pi]$ and $z_0 \in [-\pi,0]$, such that each x_0 and z_0 appears in only one pair. The pairings are randomly assigned. Numerical simulations were performed using a Runge–Kutta–Fehlberg scheme with an adaptive time-step and a maximum time step of Δt=10^{-2}.

3. Results

3.1. Non-inertial particles

In the limit of $St^{-1} \to \infty$ the motion of particles is approximated by the system

$$\frac{dx}{dt} = V_x = sin(x)cos(z), \tag{14a}$$

$$\frac{dz}{dt} = V_z = -cos(x)sin(z) - \overline{W}(t), \tag{14b}$$

where $\overline{W}(t) = W(\exp(Gt) - 1)$. We refer to Eqs. (14a) and (14b) as a *modified-Stommel model*, since Stommel (1949) investigated the motion of non-inertial particles in cellular flow when $\overline{W}(t) = W$, i.e. a time-independent constant. In Eqs. (14a) and (14b), the particle velocity at any instant is the sum of the local fluid velocity u_z and the Stokes settling velocity $\overline{W}$. The system is Hamiltonian, represented by the function $H(x, z, t) = \sin(x)\sin(z) + W(\exp(Gt) - 1)x$.

When $\overline{W} = 0$, particles behave as passive particles in Taylor-Green flow, while for $\overline{W} > 1$, particles are no longer suspended by the flow since the settling velocity dominates at all instances. For intermediate values $0 < \overline{W} < 1$, local fluid up-flow may be sufficiently strong such that some particles remain suspended in recirculation zones, but particles outside of the recirculation zone fallout. The size of the recirculation zone depends on the value of $\overline{W}$. Fig. 2(b) shows the streamlines of the Stommel model for the constant value W=0.5, with the recirculation zone outlined. In the modified-Stommel model (Eqs. (14a) and (14b)), as time increases the value of the settling velocity $\overline{W}(t)$ grows in magnitude and conditions on particle suspension and fallout change continuously. A particle's motion and fallout time depend on the governing parameters and it's initial position in the top cell. Once $t \geq (1/G)\ln(1/W + 1)$, no recirculation zone exists and all particles will settle out. We define t_f as the time it takes for a particle to fallout of the top cell, essentially

when it cross the bottom boundary $z = -\pi$ of domain Ω.

Considering the time evolution of the recirculation zone gives an insight into the statistical evolution of many particles in the early stages. At each instantaneous time t_i, the bounding curve of the recirculation zone can be computed. The streamlines of particle motion at instantaneous time t_i are constants of the Hamiltonian

$$H(x,z,t) = c = sin(x)sin(z) + W(exp(Gt_i) - 1)x \tag{15}$$

where the streamline is dependent on the value of the constant c. In the domain Ω=[0,π] × [− π,0], the streamline bounding the recirculation zone is given by

$$0 = sin(x)sin(z) + W(exp(Gt) - 1)x, \tag{16}$$

which can be rewritten as

$$z = arcsin\left(\frac{Wx(1 - exp(Gt))}{sin(x)}\right). \tag{17}$$

Function (17) is not injective, having two solutions only when

$$\left|\frac{Wx(1 - exp(Gt))}{sin(x)}\right| < 1. \tag{18}$$

In Fig. 3(a) the bounding streamline (orange) given by Eq. (17) at instantaneous times encircles the particles which are suspended by the flow from the 1000 particles randomly initiated across Ω. The particles which reside outside of the streamline at each time instant are those which are no longer suspended and are about to fall out from Ω. Individual particle paths are not shown for brevity, but for system (14) the general trend is that particles initiated closer to the cell centre drop out at later times compared to particles initiated closer to the boundary. Central particles drift with the recirculation zone, remaining suspended for the longest times.

The area of the recirculation zone can be used to determine the fraction of particles within the domain Ω that are suspended at a given time, and can be computed from

$$A(t) = 2\int_0^{x^*} arcsin\left(\frac{Wx(1 - exp(Gt))}{sin(x)}\right)\mathrm{d}x, \tag{19}$$

where x^* is the largest x for which a solution exists, which from Eq. (18) is the solution to the implicit relation $xW($ exp $(Gt) - 1) -$ sin (x)=0. Using the area $A(t)$, the ratio r_f of the cell taken up by the recirculation zone is

$$r_f(t) = \frac{\pi^2 - A(t)}{\pi^2}. \tag{20}$$

where $A(0)=\pi^2$. We compute the fallout ratio $r_f(t)$ numerically in Fig. 3 (b) for G=0.001 and 3 different values of W. The profile of r_f is the cumulative frequency of particle fallout times and differentiating r_f gives the probability distribution function PDF(t_f), the respective profiles of which are shown in (c). The PDF(t_f) is highly skewed, appears asymptotic to t=0, and non-smooth at $t = T$ such that $W($ exp $(GT) - 1)$=1. These attributes are likely due to the fact that the bounding streamline is non-smooth as seen in Fig. 2(b). For W=10 the PDF shows that a significant proportion of initial particle positions lead to suspension for many vortex turnovers before fallout. Increased suspension time near the ocean surface will lead to larger biofilm size, indicated by the respective value of N for the PDF profiles shown in Fig. 3(c). For the parameter range presented, the additional increase in N for late fallout particles is quite conservative, however, for smaller values of W and G, the biofilm can grow significantly large.

So far we have reported on the motion of particles with time dependent mass in a single cell Ω of the flow field. The results correspond to an idealised representation of system (11) with large $St^{-1} = FM/W$, which is true for microplastics in Langmuir circulation cells. The biofouled microplastics are suspended by fluid flow while the Stokes settling velocity is not greater than the velocities in upwelling regions of the flow, increasing their time spent near the ocean surface. As W decreases, in general the suspension time for particles increased. Decreasing W is equivalent in the simplest sense to decreasing the size of the microplastic particle, indicating that the smallest microplastics will remain suspended for a long time and require a large biofilm to overcome the upwelling effects of Langmuir circulations. Significant uncertainty in a particle's position can be introduced during this suspension stage, since the particle's suspension time is dependent on the particle's initial position in the flow. The amount of uncertainty is dependent on the microplastic clean rise velocity and the growth rate of the biofilm. Therefore, if fluid flow was to be ignored during modelling, there would likely be error in the prediction of a particle's vertical position in the ocean water column.

These results give a heuristic view of the behaviour which may be observed in Langmuir circulation cells, where the flow field is governed by large vortex cells in the upper ocean, aligned horizontally but only

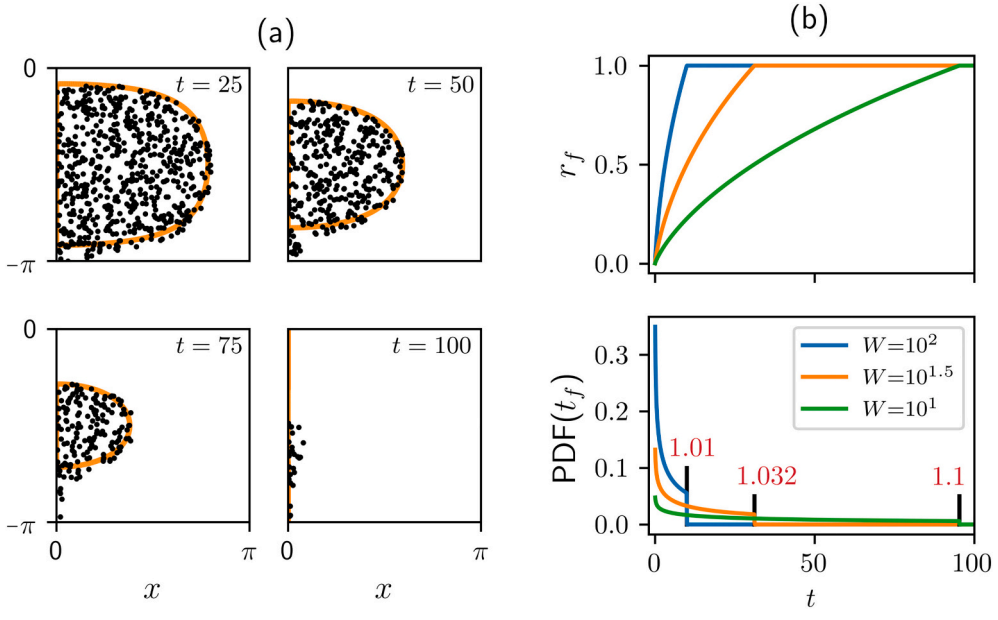

Fig. 3. (a) Snapshots at different times of the non-inertial particles which remain in Ω from the 1000 randomly initiated particles at time t=0. Particle motion is governed by the modified-Stommel model (Eqs. (14a) and (14b)) when W=10 and G=0.001. The bounding streamline of the recirculation zone (orange) encircle the particles which remain suspended at that time. (b) Ratio of particle fallout (Eq. (20)) for G=0.001 and different values of W are plotted in the upper panel. Differentiating r_f gives the PDF of fallout time for particles initiated randomly within domain Ω, lower panel. The expected values of biofilm population no. N = exp (Gt) rounded to 3 decimal places are shown in red for each W at the respective times the recirculation zone disappears. (For interpretation of the references to colour in this figure legend, the reader is referred to the web version of this article.)

one cell deep. Turbulence consists of many interacting vortices, therefore, in the vein of Maxey and Corrsin (1986) and Maxey (1987) as a first step in developing a heuristic model for particles with time dependent mass interacting with oceanic turbulence, we proceed to analyse particle motion and quantify the level of uncertainty introduced throughout vertically stacked Taylor-Green vortices. We shall add further complexity to this simple model by introducing time dependency to the velocity field later in the paper.

Since particle fallout time is dependent on (x_0, z_0) in Ω, there is uncertainty in a particle's vertical position as it continues to fall. Fig. 4 (a) plots how the range in vertical position z, across the 1000 particles uniformly initiated in Ω, evolves in time as it traverses the stacked Taylor-Green vortex cells for different values of W and G=0.001. The mean $\bar{z}$ (solid line) is shown alongside the upper and lower quartiles (extremes of dark band) and the maximum and minimum of z (extremes of the light band). We use the range (R) and inter-quartile range (IQR) as a gauge on the distribution of possible particle vertical positions, rather than say the standard deviation, since the PDF(t_f) is skewed and discontinuous (Fig. 3(b)).

There is a larger spread in the values of z for later times as W is decreased. This is shown more clearly in Fig. 4(b), which shows how the range (R) and inter-quartile range (IQR) change in time for the three values of W. The general trend for all values of W is that both R and IQR grow in time, accelerating in the beginning but decelerating once the recirculation zone disappears, marked by the solid grey line in each subplot respectively for the given W. The mean $\bar{z}$ follows exactly the analytical solution of a particle falling from $z_0 = -\pi/2$, the centre of the cell, with no flow

$$z = \frac{W}{G}(1 - exp(Gt)) + Wt - \frac{\pi}{2}. \tag{21}$$

There is a simple explanation for these observations, but since it is not integral to interpreting the remaining results, the discussion can be found in the Supporting information.

Small values of W also exhibit a larger spread in the potential vertical position of particles as they fall, due to the uncertainty in a particles trajectory depending on its initial position in the top cell. The implication of this result is that the trajectories of the smallest biofouled microplastics may be heavily influenced by their interaction with turbulent vortical flows which are non-resolved in OGCMs. In the next two sections, we perform preliminary studies on particles away from large, coherent structures and analyse the effects of particle inertia and unsteady fluid flow on the motion of biofouled microplastics as they gain mass in vortical flows.

3.2. Particles with inertia

In this section, we briefly present results on the impact of inertia for particles with time-dependent mass, when $St^{-1} = FM/W$ is finite. We expect a duel effect, in that while inertia causes particles to spin out from regions of high vorticity, the growing mass of the particles shrink recirculation zones, presenting a competition of timescales between the two mechanisms. Across the parameter ranges of interest, listed in Table 1, the Stokes number St ranges from very small (passive particles) to large values (particles dominated by inertia), although note that for certain parameter groupings the assumptions for the Maxey-Riley-Gatignol equations no longer hold, such as when W is large but F small.

An example of the initial fallout behaviour is shown in Fig. 5(a), where the bounding streamline of the recirculation zone encapsulates most of the remaining particles in Ω from the 1000 randomly initialised particles when $F=10^{2.5}$. The time snapshots and values G=0.001 and W=10 are the same as in Fig. 3(a) for non-inertial particles. In the early stages, the streamline encircles the suspended particles but as time continues the particle cluster deviates slightly from the area of the recirculation zone.

The analytic fallout ratio $r_f(t)$ (solid) from Eq. (20) is shown in Fig. 5 (b), alongside the ratio of inertial particles with different values of F, which have crossed the bottom boundary Ω from the total 1000 at a given time t (crosses). When W is large, the recirculation zone disappears quickly and particles take only a short time to cross the bottom boundary resulting in a slight shift of the cross profiles from the solid line r_f, which predicts when particles leave the recirculation zone. When W is small, the cross profiles align well with r_f and there appears to be little difference between different values of F except for the smallest value, $F=10^{2.5}$, where there is a slight increase in fallout at late times. Only when $W=10^2$ and $F=10^{2.5}$ does the inertia seem to have a noticeable difference, resulting in particles being suspended for longer. This parameter pair corresponds to large particles in cellular flows with either a small length scale or fast velocity field and are on the cusp of not being valid parameter values by the model assumptions, and so are neglected in further results.

Our results suggest that inertia has only a small impact on the suspension and initial fallout of particles, at least for the case when

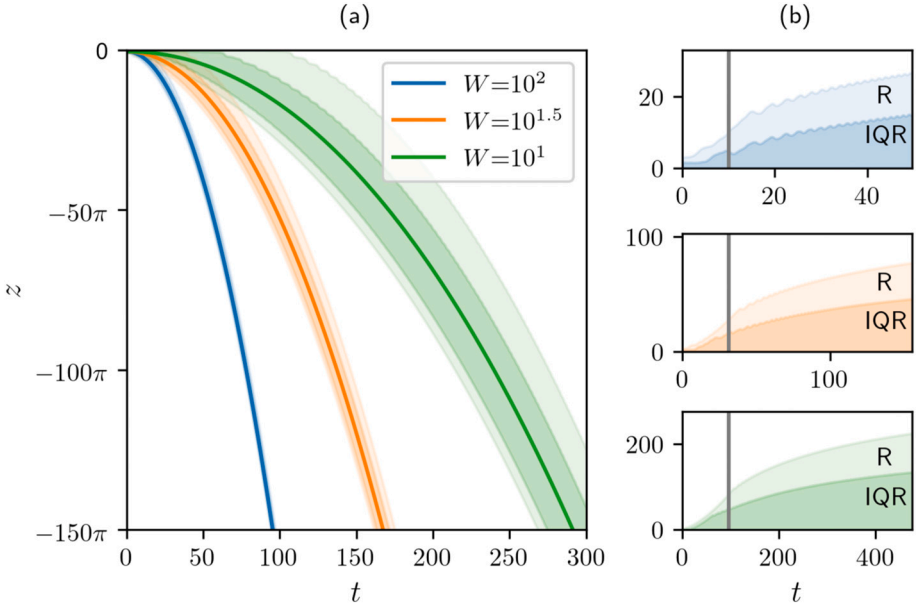

Fig. 4. (a) The time evolution of the spread in the vertical position of 1000 particles initiated in Ω is shown for three values of W and G=0.001, represented by the mean $\bar{z}$ (solid line), the inter-quartile (dark coloured band) and the range (light band). (b) The growth of the range (R) and inter-quartile range (IQR) are shown as functions of time, note the varying time-axis for different values of W. The grey vertical line indicates the time the recirculation zone disappears. (For interpretation of the references to colour in this figure legend, the reader is referred to the web version of this article.)

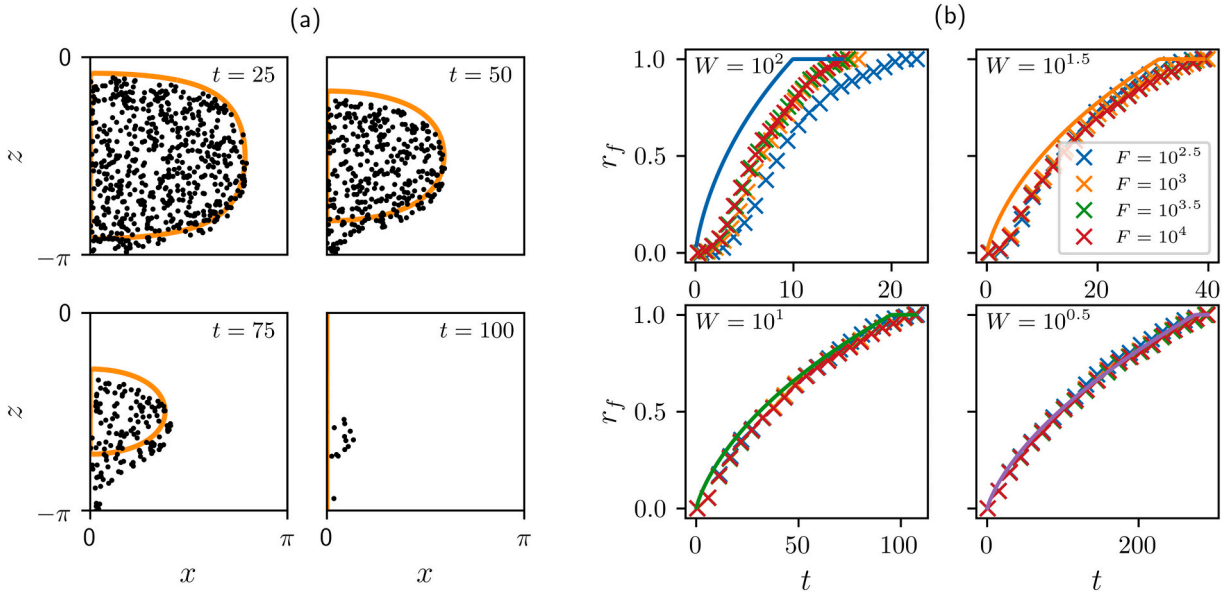

Fig. 5. (a) Snapshots at time t of the non-inertial particles which remain in Ω from the 1000 uniformly initiated at time t=0, where their motion is governed by system (11) with Taylor-Green vortex flow and when W=10, F=$10^{2.5}$ and G=0.001. The bounding streamline of the recirculation zone (orange) from the modified-Stommel model (Section 3.1) captures the particles which remain suspended. (b) The ratio of particle fallout (Eq. (20)) for different values of W and F (crosses) with G=0.001. (For interpretation of the references to colour in this figure legend, the reader is referred to the web version of this article.)

G=0.001. In this idealised flow, it may be expected that for very small values of G, that is a biofilm that grows slowly compared to vortical turnover time, that all particles settle out quicker than t=$(1/G)\ln(1/W+1)$ due to the inertial effects from their finite size. This is due to the fact that all heavy, inertial particles with fixed mass eventually settle out in vortical flows (Maxey, 1987), and for a fouled particle the timescale of inertial fallout may be quicker than the fallout from increased mass. However, in reality we would expect the life-span of a vortical turbulent structure to be much less than the timescale in which inertia is significantly impactful to suspension time.

Once particles have fallen out, the inertia impacts their settling velocities. For different value of F, Fig. 6(a) shows how the range in vertical position z evolves in time for 1000 particles uniformly initiated in Ω. When F=$10^{2.5}$ and W=10^1 (green), the mean vertical position $\bar{z}$ is slightly deeper than the analytical approximation (dashed black line), suggesting there is a speed-up in the average settling velocity due to inertial effects. This is confirmed in Fig. 7(a) which plots the relative change in the average settling velocity $\langle V_z \rangle$ compared to the

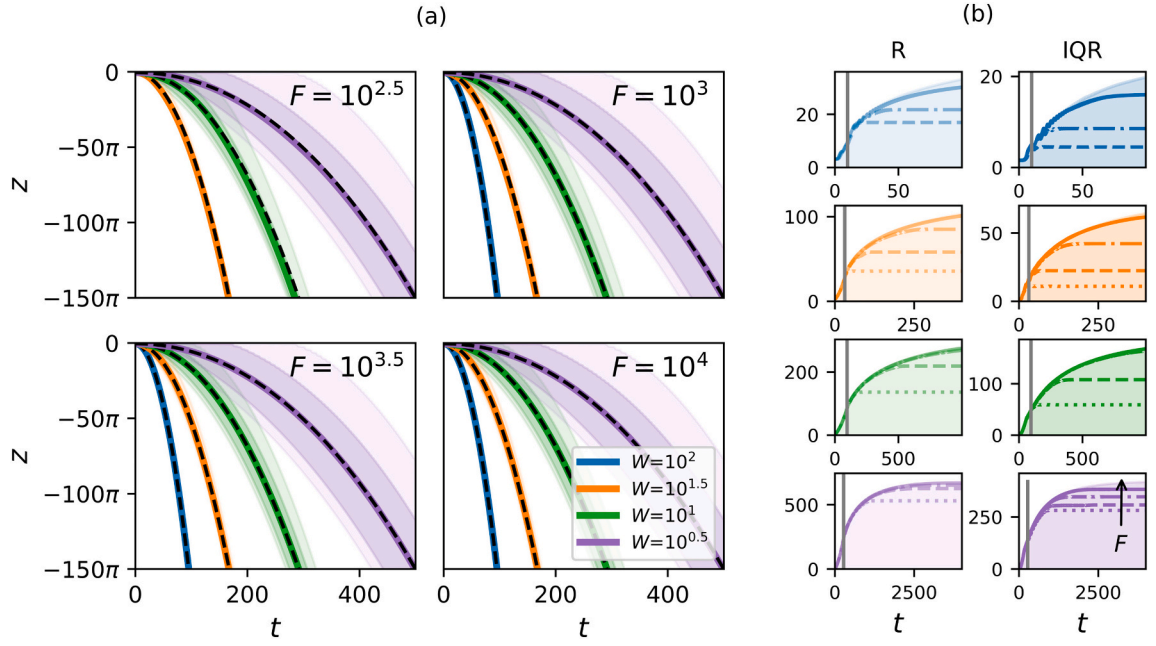

Fig. 6. (a) For different values of F, the time evolution of the spread in the vertical position of 1000 particles initiated in Ω. In each subplot, for four values of W and G=0.001, the mean $\bar{z}$ (solid line), the inter-quartile (dark coloured band) and the range (light band) are shown. The dashed black line overlays $\bar{z}$ with the analytical mean z, indicating where there is deviation (Eq. (21)). (b) The growth in the range R (LHS) and inter-quartile range IQR (RHS) shown in more detail. Values when St^{-1} is infinite (bands) is overlaid with F = $10^{2.5}$ (dotted), 10^3 (dashed) $10^{3.5}$ (dashed-dot) and 10^4 (solid). Note the varying time-axis for different values of W, the grey vertical line indicating the time T the recirculation zone disappears.

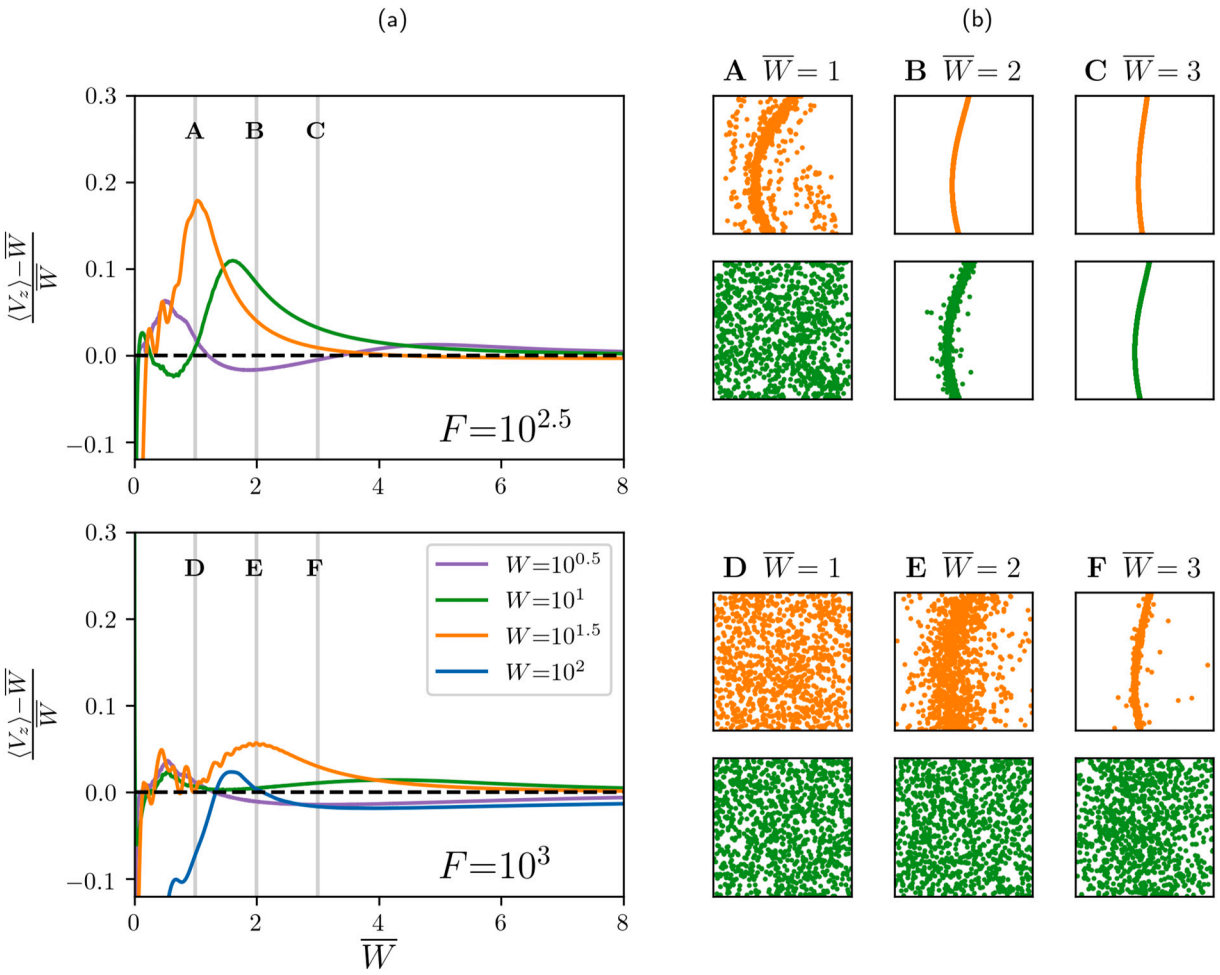

Fig. 7. (a) Relative velocity increase for inertial particles in cellular flow field shown for the two smallest values of F simulated. (b) For the two parameter values W=$10^{1.5}$ (orange) and W=10 (green) with the largest increase in average settling velocity, the 1000 particles relative position shown in one cell at the three times, when $\overline{W}$ = 1, 2 and 3, revealing clustering in fast downwelling regions is reason for speed up. (For interpretation of the references to colour in this figure legend, the reader is referred to the web version of this article.)

instantaneous Stokes settling velocity $\overline{W}$. The maximum speed up for F=$10^{2.5}$ and W=10^{1} as seen in Fig. 7(a), is only ≈10% and persists for a short window of time, when $\overline{W}$ is small. In the limit of large $\overline{W}$ the flow will have little impact on the particle motion such that $\langle V_z \rangle \to W(t)$ as $t \to \infty$. For W=$10^{1.5}$ there is a maximum relative speed up of ≈20% when F=$10^{2.5}$, which reduces to around ≈5% when F=10^{3}. The increase in average settling velocity is due to inertial particles drifting into fast downwelling regions, shown in Fig. 7(b). How particles accumulate into fast downwelling regions depends on both the value of F and W, since both contribute to the value of the Stokes number St. In Fig. 7(b), snapshots of the relative position of particles in the cells are shown at times t such that $\overline{W}(t) = W(1 - \exp(Gt))$ is equal to 1, 2 and 3. We observe that for fixed W and G, a smaller value of F results in greater accumulation of particles into downwelling regions, and the peak in the relative velocity increase profile occurs at earlier times. Physically, a smaller F can be thought of as corresponding to a cellular flow in which the cell length L is smaller or the maximum speed U_0 is higher. For example, F=10^{4} corresponds to length and velocity scales on the order of Langmuir circulation, while F=$10^{2.5}$ is closer in comparison to small-scale turbulent vortices on the order of centimetres.

In addition to increasing the settling velocity, particles drifting into downwelling regions have an additional effect in that the uncertainty in particle vertical position is reduced. Fig. 6(b) compares how range (R) and inter-quartile range (*IQR*) change in time for inertial particles and non-inertial particles. In each subplot, representing a different value of W, multiple lines are plotted for R (LHS) and *IQR* (RHS) representing different value of F. For small F, the uncertainty in vertical position stops growing as R and *IQR* become constant. This occurs relatively quickly when W is large, and shortly after the disappearance of the recirculation zone indicated by the grey vertical line. In the absence of inertia, clustering of particles is prohibited due to incompressibility of the Hamiltonian system representing particle motion (Eq. (14)). With inertia, particles drift and cluster onto fast streamlines, eventually travelling at the same velocity, thus preventing the growth of uncertainty in vertical position and it becomes constant. For each W, the rate at which clustering of particles into fast downwelling regions occurs is quicker for smaller F, and the uncertainty becomes constant at earlier times.

We assume particles are small and numbers are sparse enough that they do not affect the flow field, and simulate many particles to analyse the statistics of biofouled microplastic motion in flow rather than representing expected ocean observations. If it were true that microplastic pollution was abundant across a region of vortical cells in oceanic turbulence, the clustering mechanism could lead to a high density of particles per unit volume, which would be expected to effect the flow field or result in particle agglomeration. We do not explore these effects in the current work.

3.3. Time-dependent velocity field

The static, periodic cellular arrangement of Taylor-Green flow is a

highly idealised representation of realistic flows. A consequence of this is that for non-inertial particles governed by the modified-Stommel model, the particles which fall out at later times fall into the cell regions with the slowest average vertical velocity, while early fallout particles are destined to remain in fast downwelling regions. This leads to the distance between the early fallout and late fallout particles growing in time, even when the recirculation zone disappears and particles are no longer suspended. To understand the role unsteadiness in the flow will play in this process we follow a similar approach to (Galloway and Proctor, 1992) and consider the fallout of particles with time-dependent mass in an unsteady, cellular flow, specified by the non-dimensional streamfunction

$$\psi(x,z,t) = sin[x + Bsin(\sigma t)]sin(z). \tag{22}$$

Depending on the amplitude B and frequency σ of the sinusoidal, horizontal translation, the velocity field governed by stream function (22) causes trajectories of passive, weightless particles ($\overline{W} = 0$ and St^{-1} infinite) to partially or completely cover the domain with a chaotic sea. Details on a qualitative and quantitative assessment of the parameter space $B \in [0.5,1.0,1.5]$ and $\sigma \in [0.25,0.5,1.0]$ is left to the Supporting information, but in general mixing is enhanced for the larger values of both B and σ from these sets.

The motion of non-inertial particle centres in this unsteady flow are governed by the system

$$\frac{dx}{dt} = sin[x + Bsin(\sigma t)]cos(z), \quad \frac{dz}{dt} = cos[x + Bsin(\sigma t)]sin(z) - \overline{W}(t), \tag{23}$$

again taking $\overline{W}(t) = W(\exp(Gt) - 1)$. For any (B, σ) and when $0 < \overline{W}(t) < 1$ the recirculation zone area r_f is the same for Eqs. (14a) and (14b), ensuring a direct comparison of the results in earlier sections can be made. This is not the case for other simple unsteady cellular flows, such as that investigated by (Smith and Spieqel, 1985) given by the stream function $\psi(x, z, t) = [1 + \varepsilon \sin(\omega(t))] \sin(x) \sin(z)$, which has a pulsed amplitude in the magnitude of maximum velocity.

In this time-dependent flow, fallout times for particles initiated across Ω are reduced even though the shrinking rate of the recirculation zone is the same as for the steady, modified Stommel model. The times are significantly reduced for the larger values of B and σ. This is due to the fact that particles are not restricted to re-suspension only in the first cell when the flow field is unsteady; they are able to fallout and become re-suspended for some time in lower cells (Fig. S2 in the Supporting information).

The unsteady flow field has a large impact on the statistics of particle vertical position, shown in Fig. 8. The mean $\bar{z}$, shown for $(B, \sigma) = (1.5,0.25)$ in Fig. 8(a), is again overlapped by the expected analytic expression (21) (dashed black line). In comparison to when the flow is steady, the range R and inter-quartile range *IQR* in the unsteady flow are reduced across every value of W. In Fig. 8(b) the time-evolution of the range and inter-quartile range in the unsteady flow field with $(B, \sigma) = (1.5,0.25)$ (solid lines) are overlaid the evolution of their values in the steady flow field (filled bands). When $W=10^2$ the range in particle vertical position in the unsteady flow continues to grow at a range similar to steady flow, until just after the recirculation zone disappears and then becomes almost constant. The growth in the range when $W=10^{1.5}$ and 10 is qualitatively similar, appearing to plateau once the recirculation zone has, or is close-to, disappearing. When $W=10^2$ and $10^{1.5}$, the inter-quartile range has a similar fate to the range, whereas for $W=10$ the inter-quartile range is significantly reduced in value from very early times.

The reduction in the uncertainty of particle vertical position when the flow is unsteady is due to two mechanisms. The first being that re-suspension of particles is not limited to the top cell and is possible throughout the vertical column while the recirculation zone is in existence. Therefore, the range is no longer bounded as in steady flow, by the particle which falls out first and the last suspended particle which is trapped in the top cell, but rather the particles whose trajectories have traversed the most and least number of cells from motion driven by fallout and re-suspension. Secondly, in the modified-Stommel model particles which fall out early surf in fast down-welling regions for all remaining times due to the arrangement of the cells. In the unsteady flow, particles interact with a wider range of fluid velocities, meaning on average the early fallout particles fall slower than their steady flow counterparts, and late fallout particles move quicker than their steady flow counterparts. The latter mechanism is the reason for the plateau in the growth of uncertainty once the recirculation zone disappears.

Fig. 8(c) compares the time evolution of the range R and inter-quartile range *IQR* across W and B, where different lines on each plot represent different values of σ. All values of B and σ shown produce a reduction in the uncertainty of particle position. Small B is not effective

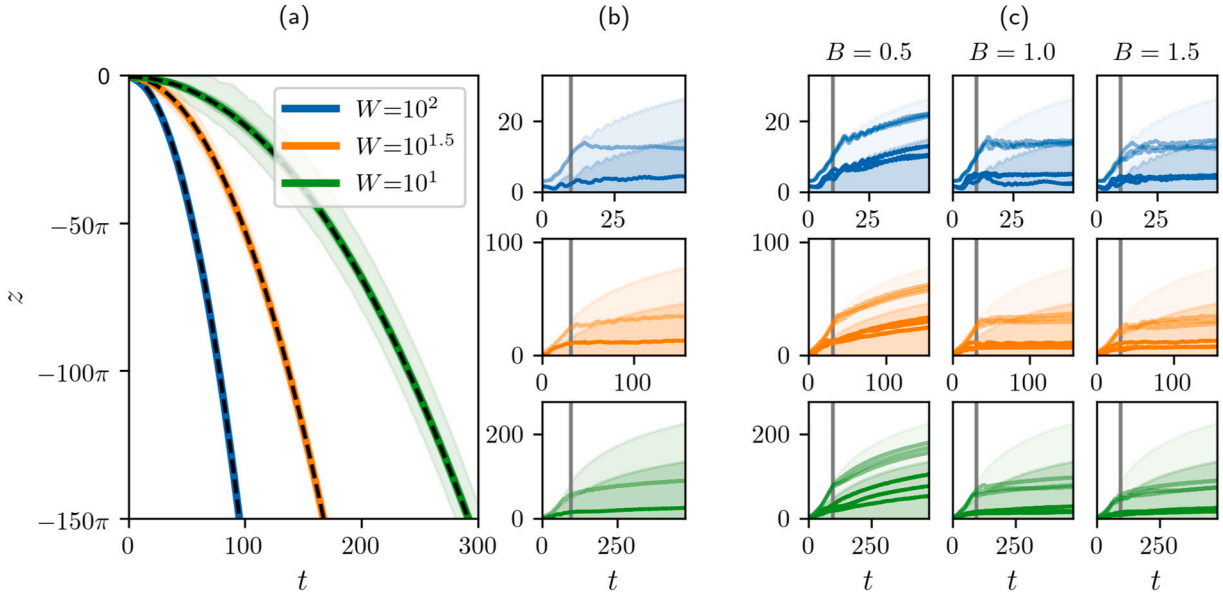

Fig. 8. (a) The time evolution of the spread in the vertical position of 1000 particles initiated in Ω governed by system (23) with B=1.5 and σ=0.25. (b) The growth of the range (R) and inter-quartile range (*IQR*) in time when B=1.5 and σ=0.25. (c) The growth in the R and *IQR* are shown in different plots for W and B, with the multiple lines representing different values of σ. The grey vertical line indicates the time the recirculation zone disappears. In all G=0.001.

at reducing uncertainty, instead the uncertainty keeps growing after the recirculation zone disappears, potentially due to the fact that the small amplitude in the cell translation means falling particles do not interact with a velocity field as varied as when B is large. For large enough values (B, σ), the plateau appears almost independent of the parameters governing flow translation.

In Section 3.2, we saw that clustering of inertial particles in steady flow also resulted in a plateau for the growth of uncertainty in particle vertical position, but this was due to clustering into fast downwelling regions where eventually every particle is falling at the same time-dependent average velocity along a single trajectory. The time-scale at which the clustering takes place is dependent on the value F, which parameterises the Stokes number for a given W. We conclude the study of this subsection by analysing the motion of inertial particles in unsteady flow fields.

Fig. 9 plots the vertical position statistics for 1000 inertial particles uniformly initiated in Ω. In Fig. 9(a) the mean $\bar{z}$, range R and inter-quartile range IQR are shown for different values of F and W, for the singular pair $(B, \sigma) = (1.5, 0.25)$. In all profiles, the mean appears to align well with the analytic mean of the modified-Stommel model (21) (black-dashed), while the range R and inter-quartile range IQR are once again significantly reduced. Fig. 9(b) plots the growth in time of the range R and interquartile range IQR across values of W, B and fixed σ. In each plot, lines representing different values of F are overlaid profiles from the steady modified-Stommel model (bands). When B=0.5, all profiles for both R and IQR differ from the steady modified-Stommel model and are dependent on the value of F, as was seen for inertial particles in steady flow in Fig. 6. However, for larger B the profiles all plateau at early times, close to when the recirculation zone disappears, and appear independent of F suggesting that the effect of unsteady flow may be more important than the effects of inertia in the system. The results look qualitatively similar for the two values σ=0.5 and 1.0, excluded for brevity. We confirm that no significant speed up in the mean vertical velocity profile at intermediate times is observed in comparison to the analytical mean (Eq. (21)), shown in Supporting information Fig. S3, even though clustering of particles still occurs but to a lesser degree.

3.4. Uncertainty parameter scaling

We have established that simple vortical flows, used as idealistic representations of the vortical structures in turbulence, introduce uncertainty in the trajectories of biofouled microplastic. The level of uncertainty is governed by parameters defined from both flow and microplastic properties. Parameterisations of turbulence using eddy diffusivity are independent of the latter (Jalón-Rojas et al., 2019; Fischer et al., 2022). In this final results section we quantify, in dimensional space, the uncertainty in the vertical position of biofouled microplastics introduced by Taylor-Green flow across dimensional parameter ranges for microplastics in chaotic flow fields.

When the vortical flow is steady, both the range R and inter-quartile range IQR increase in value over time, with the fastest growth occurring prior to the recirculation zone disappearing. For non-inertial particles, we attribute the continued growth in uncertainty to the idealised, static arrangement of the steady vortical cells where early fallout particles remain on fast downward trajectories while late fallout out particles are destined to remain on the slowest. All inertial particles eventually cluster onto fast downwelling trajectories, although the effect on the particle vertical position distribution happens largely after the recirculation zone has disappeared. This behaviour contrasts the unsteady flow, where for well-mixed, time-dependent flow fields the growth in uncertainty of particle vertical position mostly increases prior to the recirculation zone disappearing and only a minimal increase in the values of R and IQR occur at later times. This was irrespective of particle inertia. Therefore, as a single measure to interpolate the expected uncertainty across parameter ranges, we adopt the functional form $IQR_T \equiv QR(T)$ as a metric, where T is the time the recirculation zone disappears.

For steady Taylor-Green flow, Fig. 10(a) shows how the values of IQR_T depend on W and G from numerical simulation of 1000 non-inertial particles with time dependent mass (squares). The data closely follows a power-law scaling for both W and G of $IQR_T = CG^{\eta}W^{\zeta}$, where exponents η, ζ, and constant C are determine numerically. The solid lines in Fig. 10 show the scaling

$$IQR_T = 0.4G^{-1}W^{-0.92}, \tag{24}$$

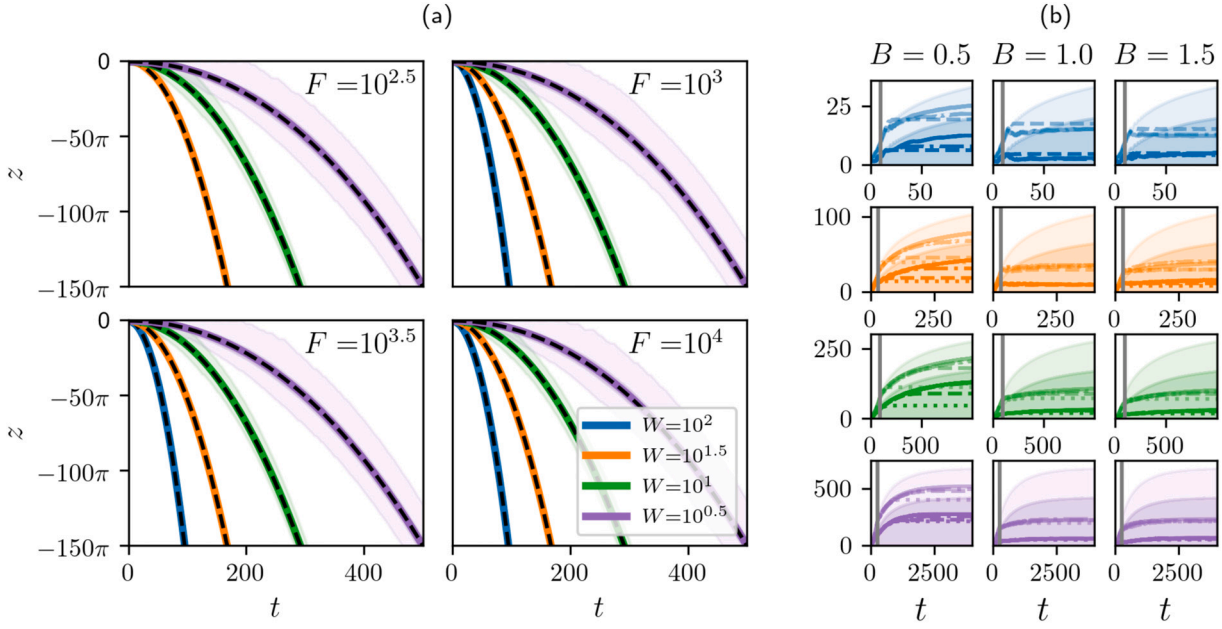

Fig. 9. (a) Subplots for different F showing the time evolution of the spread in the vertical position of 1000 particles initiated in Ω governed by the modified-Maxey model with time-dependent velocity field. (b) The growth of the range (R) and inter-quartile range (IQR) in time when σ=0.25 and different values of B. Different lines correspond to different values of F. The uncertainty in the vertical position of particles is greatly reduced and almost independent of F when B is large enough. In all G=0.001.

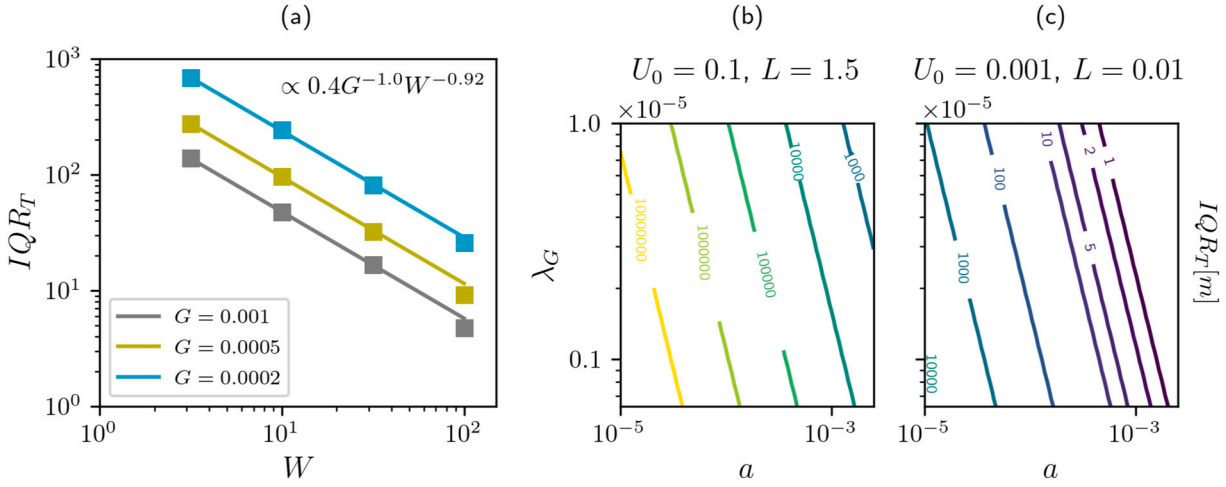

Fig. 10. (a) The inter-quartile range at the time the recirculation zone disappears, IQR_T, is plotted for different values of W and G (squares). The power-law scaling (24) approximated from the data is overlaid (solid lines) showing good agreement. In (b, c) the power-law scaling is used to contour IQR_T in metres [m] for vertical flows with U_0 and L on the order of (b) Langmuir circulation and (c) small-scale turbulent vortices on the order of a centimetre taking ε=10^{-3}. The contour lines are expressed across dimensional quantities of particle radius a and biofilm growth rate λ_G, and assuming fixed, mid-range values for the other parameters μ=10^{-3} [kg·m^{-1}·s^{-1}], ρ_f=1025 [kg·m^{-3}], ρ_p=900 [kg·m^{-3}] and g=9.8 [m·s^{-2}] given in Table 1.

found using a least-squares approximation to function fit the data (squares), showing good agreement with the simulation results. For [C, η, ζ] the standard deviation in parameter estimation error was respectively [0.019,0.0056,0.0051]. We use relation (24) to estimate the uncertainty for dimensional vortical flows on the length and timescales of oceanic turbulence, extrapolating to parameter ranges beyond the means of simulation.

For the parameter ranges of interest given in Table 1 concerning biofouled microplastics in the ocean, particle radii a vary over orders of magnitude whereas the differences between seawater and microplastic densities ($\rho_f - \rho_{mp}$), dynamic viscosity of seawater μ, and gravitational acceleration g vary little or not at all in comparison. The variation of the dimensionless parameter W is mainly governed by the value of a and the maximum speed of vertical cells U_0. For the dimensionless parameter G: U_0, L and λ_G all vary over an order of magnitude or more. For a given U_0 and L, corresponding to a vortical cell expected in oceanic turbulence, we ask how IQR_T [m] changes depending on a and λ_G from relation (25). We fix ρ_f=1025 kg·m^{-3}, ρ_{mp}=900 kg·m^{-3}, μ=10^{-3} kg·m^{-1}·s^{-1} and g=9.8 m·s^{-2} as mid-range values of the parameters in Table 1.

Contours of IQR_T [m] are shown in Fig. 10(b, c) on a logarithmic scale for cellular flows representative of different vortical cells of oceanic turbulence. In (b) the contours quantify the uncertainty for U_0=0.1 m·s^{-1} and L=1.5 m, typical scales for Langmuir circulation with a cell height of ≈4.7m, and in (c) for U_0=0.001 m·s^{-1} and L=0.01 m, corresponding to turbulent vortices on the length-scale of a centimetre and a turbulent energy dissipation rate ε=0.001 cm^2·s^{-3}. In (b) values of IQR_T [m] range from hundreds to over millions of metres across the ranges of a and λ_G, the top range being over 100 times deeper than the ocean at its largest depths. For small radii a, the excess values are due to the fact that late-fallout out particles, initiated central to the vortical cell, would need to be suspended for a very long time and acquire an extremely large biofilm to overcome the fast, upwelling velocity. There are also other factors in these unrealistic values of IQR_T [m]. Firstly, Taylor-Green vortices are not representative of real oceanic turbulent flows, neglecting their multi-scale nature. Particles trapped for long-times in the top cell of the simulation, which we defined close to the ocean surface, would likely experience a different fate in the ocean following a more chaotic trajectory as they traverse many multi-scale vortices, which steady Taylor-Green cellular flow is unable to capture. Secondly, we model the biofilm as having fixed, exponential growth which is a great simplification of the biological process since growth rate variation with depth would be expected due to changing environmental conditions and the plastic particle may have an upper bound on the biofilm it can support, or indeed the limitations of the model to estimate the particle hydrodynamics once the biofilm is large. In Fig. 10(c), representing turbulent vortices on the length-scale of centimetres, the values of IQR_T are significantly less than in (b) but they are still large for the smallest values of a, and unrealistic due to the same arguments made above.

Introducing a time-dependent, horizontal translation to Taylor-Green flow introduces the potential for chaotic particle paths, a small-step away from the idealistic steady flow. For unsteady Taylor-Green flow, Fig. 11(a) shows how the values of IQR_T depend on W and G from numerical simulation of 1000 non-inertial particles with time dependent mass. The mean (squares) and the maximum/minimum (whiskers) values of IQR_T are shown for parameter pairs (B, σ) with $B \in$ [1.0,1.5] and $\sigma \in$ [0.25,0.5,1.0], parameterising the unsteady flow. Fitting to the mean values of IQR_T, a power-law scaling

$$IQR_T = 0.62G^{-0.63}W^{-0.58}, \tag{25}$$

is found (solid lines), again showing good agreement. For [C, η, ζ] the standard deviation in parameter estimation error was respectively [0.062,0.012,0.009]. Fig. 11(b, c) shows IQR_T [m] using the scaling relation (25) across the same parameter ranges as Fig. 10(b, c), except now the range in values of IQR_T [m] are significantly reduced. However, for the case U_0=0.1 m.s^{-1} and L=1.5 m in Fig. 11(b) the inter-quartile range can vary between roughly 100–10,000 m, showing that vortical flows have the potential to introduce large uncertainty to a biofouled microplastics position in the ocean water column. While unsteady Taylor-Green flow is still an idealised representation of turbulent flows, most notably neglecting the interaction of multiple spatial scales which will increase mixing, the results indicate that neglecting the true impact of background fluid flow when modelling the trajectories of fouled microplastics could lead to large deviations from their true transport within the ocean.

4. Conclusions

Our results show that in the early stages of biofouling, microplastic-biofilm aggregates are susceptible to continued suspension in up-welling regions of simple vortical flow, even if they are negatively buoyant compared to the surrounding fluid. As the mass increases, the

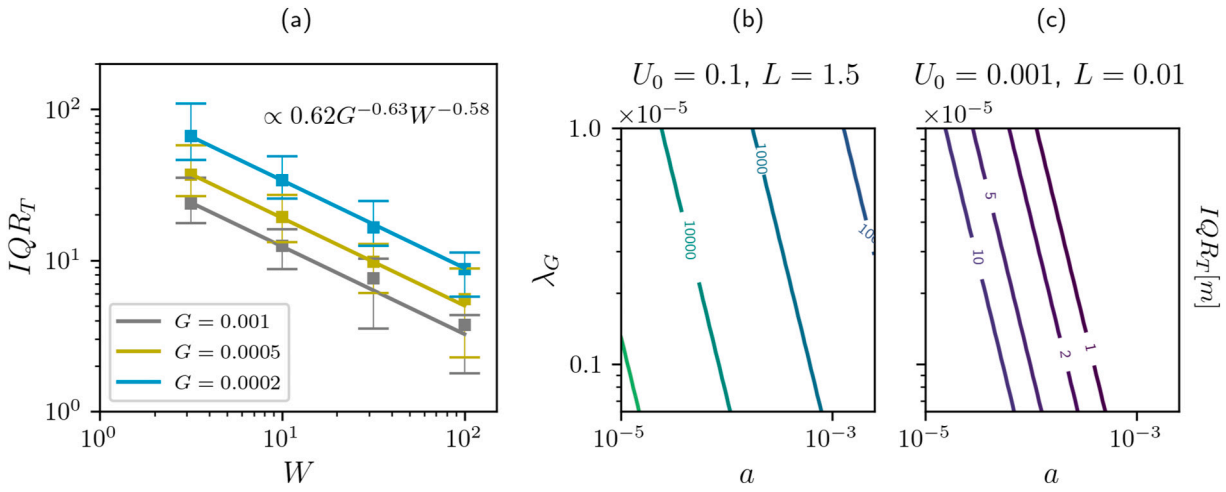

Fig. 11. (a) The inter-quartile range at the time the recirculation zone disappears, IQR_T, is plotted for different values of W and G (squares). The power-law scaling (25) approximated from the data is overlaid (solid lines) showing good agreement. In (b, c) the power-law scaling is used to contour IQR_T in metres [m] for vortical flows with U_0 and L on the order of (b) Langmuir circulation and (c) small-scale turbulent vortices on the order of a centimetre taking ε=10^{-3}. The contour lines are expressed across dimensional quantities of particle radius a and biofilm growth rate λ_G, and assuming fixed, mid-range values for the other parameters μ=10^{-3} [kg·m^{-1}·s^{-1}], ρ_f=1025 [kg·m^{-3}], ρ_p=900 [kg·m^{-3}] and g=9.8 [m·s^{-2}] given in Table 1.

recirculation zone in which they are trapped shrinks until it eventually disappears. The suspension time of an individual aggregate is dependent on microplastic, biofilm, and flow field characteristics and the aggregate's position within the vortical cell when it achieves neutral buoyancy. The latter fact introduces long-time uncertainty in a particle's trajectory through the ocean vertical water column since its initial position in the flow is not known. For the idealised 'test' flows presented here, the distribution of fallout times is non-uniform with a significant proportion of aggregate particle initial positions resulting in long-suspension times in comparison to the mean. Fallout time distributions with the largest spread were observed for the smallest microplastic particles in steady, vortical flows with length and velocity scales on the order comparable to Langmuir circulations. If the flow is unsteady, trajectory uncertainty can still be significant but the range in fallout time distributions is significantly reduced. Inertia of particles is found to have a minimal effect in reducing uncertainty introduced by flow suspension in the early stages, but for intermediate times a slight increase in the settling velocity is possible due to the fact that particles accumulate in regions in which the rate at which they pass through the vortical cells is fastest. This inertial-induced increase in velocity is greater for parameters representing vortices on the order of centimetres, comparable to small-scale fluctuations in oceanic turbulence, although still small enough that it could be reasonably neglected in parametrisations of subgrid turbulence, but further work is needed to address this.

Our motivation was to investigate the impact of vortical flows, characteristic of oceanic turbulence, on the trajectories of biofouled microplastics. Currently, modelling efforts to track the transport of biofouled microplastics using OGCMs cannot explicitly represent 3-dimensional turbulence due to limitations in computational power. Instead, turbulence is parameterised by horizontal and vertical eddy diffusivities, the latter often depending on local flow stability. This misses a key finding of this work, that microplastic aggregates can experience a prolonged suspension in the wind-mixed layer of the ocean. They would then occupy a longer period of time close to the ocean surface and thus a larger biofilm than if no flow was present. In contrast, if the vortical flows submerge aggregate particles quicker than expected, the biofilm may be reduced; both would affect aggregate buoyancy. Uncertainty in an aggregate's density and position at a given time would have long-time implications on its sinking and advection in the ocean. Neglecting, or misrepresentation, of this uncertainty could lead to predictive errors when using OGCMs in an attempt to forecast global distribution of subsurface microplastics that have sunk due to biofouling. Current parametrisations of the uncertainty introduced via eddy diffusivity coefficients are independent of aggregate characteristics, while our results suggest these are important in how the particles interact with the background flow.

The largest range in the uncertainty of suspension time introduced by idealised vortical flow is for those with flow characteristics comparable to Langmuir circulation cells. Although Langmuir circulations are not stacked cellular flows like Taylor Green, they are powerful flows with strong upwelling velocities leading to suspension of organic matter in the ocean (Thorpe, 2004). We found that for unsteady flow, inertial particles persisted to cluster into favoured regions in the cells, which may lead to particle agglomeration if microplastic-biofilm aggregate concentration is sufficiently high within several interacting eddies in a wind-mixed ocean layer. Agglomeration between particles could significantly change particle motion compared to individual particles. Further investigation into any of these aforementioned physical-biological processes towards a more realistic representation of biofouled microplastics in turbulent flows will lead to increased understanding of their motion in the ocean. In turn, this will facilitate parameterisations for the sinking rate of biofouled microplastic for adoption in OGCMs where ocean turbulence is unresolved.

CRediT authorship contribution statement

Hannah Kreczak: Conceptualization, Methodology, Formal analysis, Writing – original draft, Funding acquisition. **Andrew W. Baggaley:** Conceptualization, Methodology, Writing – review & editing. **Andrew J. Willmott:** Conceptualization, Methodology, Writing – review & editing.

Declaration of competing interest

The authors declare that they have no known competing financial interests or personal relationships that could have appeared to influence the work reported in this paper.

Data availability

No data was used for the research described in the article.

Acknowledgments

HK was funded by the EPSRC Doctoral Prize Fellowship under grant EP/R51309X/1. This research has been partly funded through the UKRI-NERC project CAMPUS (Combining Autonomous observations and Models for Predicting and Understanding Shelf seas) under grant NE/R006776/1 awarded to AJW.

Appendix A. Supplementary data

Supplementary data to this article can be found online at https://doi.org/10.1016/j.marpolbul.2023.114729.

References

Andrady, A.L., 2011. Microplastics in the marine environment. Mar. Pollut. Bull. 62, 1596.
Avio, C.G., Gorbi, S., Regoli, F., 2017. Plastics and microplastics in the oceans: from emerging pollutants to emerged threat. Mar. Environ. Res. 128, 2.
Chen, X., Xiong, X., Jiang, X., Shi, H., Wu, C., 2019. Sinking of floating plastic debris caused by biofilm development in a freshwater lake. Chemosphere 222, 856.
Cole, M., Lindeque, P., Fileman, E., Halsband, C., Goodhead, R., Moger, J., Galloway, T. S., 2013. Microplastic ingestion by zooplankton. Environ.Sci.Technol. 47, 6646.
Cózar, A., Echevarría, F., González-Gordillo, J.I., Irigoien, X., Úbeda, B., Hernández-León, S., Palma, Á.T., Navarro, S., García-de Lomas, J., Ruiz, A., et al., 2014. Plastic debris in the open ocean. Proc. Natl. Acad. Sci. 111, 10239.
Davison, S.M., White, M.P., Pahl, S., Taylor, T., Fielding, K., Roberts, B.R., Economou, T., McMeel, O., Kellett, P., Fleming, L.E., 2021. Public concern about, and desire for research into, the human health effects of marine plastic pollution: results from a 15-country survey across Europe and Australia. Glob. Environ. Chang., 102309
Eriksen, M., Lebreton, L.C., Carson, H.S., Thiel, M., Moore, C.J., Borerro, J.C., Galgani, F., Ryan, P.G., Reisser, J., 2014. Plastic pollution in the world's oceans: more than 5 trillion plastic pieces weighing over 250,000 tons afloat at sea. PloS One 9, e111913.
Fazey, F.M., Ryan, P.G., 2016. Biofouling on buoyant marine plastics: an experimental study into the effect of size on surface longevity. Environ. Pollut. 210, 354.
Fischer, R., Lobelle, D., Kooi, M., Koelmans, A., Onink, V., Laufkötter, C., Amaral-Zettler, L., Yool, A., van Sebille, E., 2022. Modelling submerged biofouled microplastics and their vertical trajectories. Biogeosciences 19, 2211.
Galloway, D.J., Proctor, M.R., 1992. Numerical calculations of fast dynamos in smooth velocity fields with realistic diffusion. Nature 356, 691.
Gatignol, R., 1983. The faxen formulae for a rigid particle in an unsteady non-uniform stokes flow. J.Méc.Théor.Appl. 143.
Int-Veen, I., Nogueira, P., Isigkeit, J., Hanel, R., Kammann, U., 2021. Positively buoyant but sinking: polymer identification and composition of marine litter at the seafloor of the North Sea and Baltic Sea. Mar. Pollut. Bull. 172, 112876.
Jalón-Rojas, I., Wang, X.H., Fredj, E., 2019. A 3d numerical model to track marine plastic debris (trackmpd): sensitivity of microplastic trajectories and fates to particle dynamical properties and physical processes. Mar. Pollut. Bull. 141, 256.
Kaiser, D., Kowalski, N., Waniek, J.J., 2017. Effects of biofouling on the sinking behavior of microplastics. Environ. Res. Lett. 12, 124003.
Kooi, M., Nes, E.H.v., Scheffer, M., Koelmans, A.A., 2017. Ups and downs in the ocean: effects of biofouling on vertical transport of microplastics. Environ.Sci.Technol. 51, 7963.
Kreczak, H., Willmott, A.J., Baggaley, A.W., 2021. Subsurface dynamics of buoyant microplastics subject to algal biofouling. Limnol. Oceanogr. 66, 3287–3299.
Kvale, K., Prowe, A., Chien, C.T., Landolfi, A., Oschlies, A., 2020. The global biological microplastic particle sink. Sci. Rep. 10, 1.
Lagarde, F., Olivier, O., Zanella, M., Daniel, P., Hiard, S., Caruso, A., 2016. Microplastic interactions with freshwater microalgae: hetero-aggregation and changes in plastic density appear strongly dependent on polymer type. Environ. Pollut. 215, 331.
Leibovich, S., 1983. The form and dynamics of Langmuir circulations. Annu. Rev. Fluid Mech. 15, 391.
Li, S., Li, M., Gerbi, G.P., Song, J.-B., 2013. Roles of breaking waves and Langmuir circulation in the surface boundary layer of a coastal ocean. J.Geophys.Res.Oceans 118, 5173.
Li, D., Liu, K., Li, C., Peng, G., Andrady, A.L., Wu, T., Zhang, Z., Wang, X., Song, Z., Zong, C., et al., 2020. Profiling the vertical transport of microplastics in the West Pacific Ocean and the East Indian Ocean with a novel in situ filtration technique. Environ.Sci.Technol. 54, 12979.
Lobelle, D., Kooi, M., Koelmans, A.A., Laufkötter, C., Jongedijk, C.E., Kehl, C., van Sebille, E., 2021. Global modeled sinking characteristics of biofouled microplastic. J. Geophys.Res.Oceans 126.
Maxey, M.R., 1987. The motion of small spherical particles in a cellular flow field. Phys. Fluids 30, 1915.
Maxey, M.R., Corrsin, S., 1986. Gravitational settling of aerosol particles in randomly oriented cellular flow fields. J.Atmos.Sci. 43, 1112.
Maxey, M.R., Riley, J.J., 1983. Equation of motion for a small rigid sphere in a nonuniform flow. Phys.Fluids 26, 883.
Michels, J., Stippkugel, A., Lenz, M., Wirtz, K., Engel, A., 2018. Rapid aggregation of biofilm-covered microplastics with marine biogenic particles. Proc. R. Soc. B 285, 20181203.
Mountford, A.S., Morales Maqueda, M.A., 2019. Eulerian modeling of the three-dimensional distribution of seven popular microplastic types in the global ocean. J. Geophys.Res.Oceans 124, 8558.
Napper, I.E., Thompson, R.C., 2020. Plastic debris in the marine environment: history and future challenges. Global Chall. 4, 1900081.
Porter, A., Lyons, B.P., Galloway, T.S., Lewis, C., 2018. Role of marine snows in microplastic fate and bioavailability. Environ.Sci.Technol. 52, 7111.
Rummel, C.D., Jahnke, A., Gorokhova, E., Kühnel, D., Schmitt-Jansen, M., 2017. Impacts of biofilm formation on the fate and potential effects of microplastic in the aquatic environment. Environ.Sci.Technol.Lett. 4, 258.
Salta, M., Wharton, J.A., Blache, Y., Stokes, K.R., Briand, J.-F., 2013. Marine biofilms on artificial surfaces: structure and dynamics. Environ. Microbiol. 15, 2879.
Smith, L.A., Spieqel, E.A., 1985. Pattern formation by particles settling in viscous flows. In: Macroscopic Modelling of Turbulent Flows. Springer, pp. 306–318.
Stommel, H., 1949. Trajectories of small bodies sinking slowly through convection cells. J. Mar. Res. 8, 24.
Talley, L.D., 2011. Descriptive Physical Oceanography: An Introduction. Academic Press.
Thorpe, S.A., 2004. Langmuir circulation. Annu. Rev. Fluid Mech. 36, 55.
Van Melkebeke, M., Janssen, C., De Meester, S., 2020. Characteristics and sinking behavior of typical microplastics including the potential effect of biofouling: implications for remediation. Environ.Sc.Technol. 54, 8668.
Van Sebille, E., Wilcox, C., Lebreton, L., Maximenko, N., Hardesty, B.D., Van Franeker, J. A., Eriksen, M., Siegel, D., Galgani, F., Law, K.L., 2015. A global inventory of small floating plastic debris. Environ. Res. Lett. 10, 124006.
Van Sebille, E., Aliani, S., Law, K.L., Maximenko, N., Alsina, J.M., Bagaev, A., Bergmann, M., Chapron, B., Chubarenko, I., Cózar, A., et al., 2020. The physical oceanography of the transport of floating marine debris. Environ. Res. Lett. 15, 023003.
Wang, L.-P., Maxey, M.R., 1993. Settling velocity and concentration distribution of heavy particles in homogeneous isotropic turbulence. J. Fluid Mech. 256, 27.
Wright, S.L., Thompson, R.C., Galloway, T.S., 2013. The physical impacts of microplastics on marine organisms: a review. Environ. Pollut. 178, 483.
Ye, S., Andrady, A.L., 1991. Fouling of floating plastic debris under biscayne bay exposure conditions. Mar. Pollut. Bull. 22, 608.